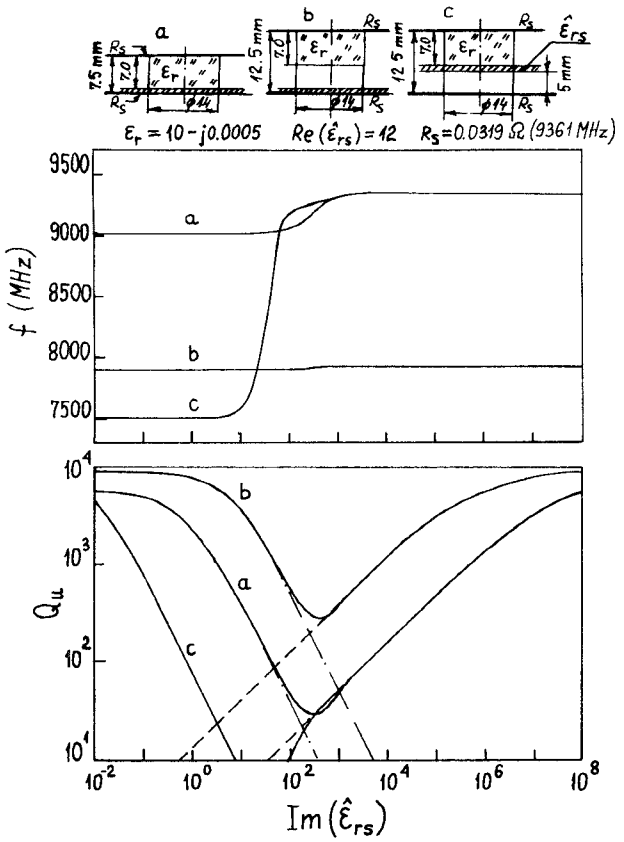

Fig. 6. $TE_{01\delta}$-mode frequencies and unloaded Q_u-factor values versus the imaginary part of substrate permittivity $\mathrm{Im}(\epsilon_{rs})$. The results have been obtained by means of the complex mode-matching method with $N = 5$. Dashed lines indicate Q_u-factor values computed by means of perturbation theory with real mode-matching method.

small. For the systems considered in Fig. 6, a small $\mathrm{Im}(\epsilon_{rs})$ value means any value smaller than 1. As is seen, only in relatively narrow ranges of $\mathrm{Im}(\epsilon_{rs})$ must complex frequency formalism be used for the resonant frequency and Q_u-factor computations.

References

[1] U. Crombach and R. Michelfeit, "Rezonanzfrequenzen and Feldstarken in geschirmten dielektrischen Sheiben und Ringresonatoren," *Frequenz*, vol. 35, no. 12, pp. 324–328, 1981

[2] Y. Kobayashi, N. Fukuoka, and S. Yoshida, "Resonant modes for a shielded dielectric rod resonator," *Electronics and Communication in Japan*, vol. 64-B, no. 11, pp. 46–51, 1981.

[3] Y. Kobayashi, T. Aoki, and Y. Kabe, "Influence of conductor shields on the Q-factors of a TE_0 dielectric resonator," in *IEEE MTT-S Int. Microwave Symp. Dig.* (St. Louis), June 1985, pp. 281–284.

[4] J. Krupka and Sz. Maj, "Application of $TE_{01\delta}$ mode dielectric resonator for the complex permittivity measurements of semiconductors," in *CPEM'86 Conf. Dig.* (Gaithersburg), June 23–27, 1986, pp. 154–155.

[5] F. H. Gil and J. Gisermo, "Finite element analysis of dielectric resonators on microstrip structures," in *Proc. XXIst General Assembly of URSI* (Florence, Italy), Aug. 28–Sept. 5, 1984.

[6] P. S. Kooi, M. S. Leong, and A. L. S Prakash, "Finite element analysis of the shielded cylindrical dielectric resonator," *Proc. Inst. Elec. Eng.*, pt. H, vol. 132, pp. 7–16, Feb. 1985.

[7] J. Delaballe, P. Guillon, and Y. Garault, "Local complex permittivity measurement on MIC substrates," *Arch. Elek. Ubertragung.*, vol. 35, no. 2, pp. 80–83, 1981.

[8] J Krupka, "Optimization of an electrodynamic basis for determination of the resonant frequencies of microwave cavities partially filled with a dielectric," *IEEE Trans. Microwave Theory Tech.*, vol MTT-31, pp. 302–305, Mar. 1983.

[9] J. Krupka, "Computations of frequencies and intrinsic Q-factors of TE_{0nm} modes of dielectric resonators," *IEEE Trans. Microwave Theory Tech.*, vol. MTT-33, pp. 274–277, Mar. 1985.

[10] D. Kajfez and P. Guillon, *Dielectric Resonators*. Dedham, MA: Artech House, 1986, ch. 7.

[11] D. Kajfez, "Incremental frequency rule for computing the Q-factor of a shielded TE_{0mp} dielectric resonator," *IEEE Trans. Microwave Theory Tech.*, vol. MTT-32, pp. 941–943, Aug. 1984.

[12] N. Imai and K. Yamamoto, "A design of high-Q dielectric resonators for MIC applications," *Electronics and Communications in Japan*, vol 67-B, pp. 59–67, Dec. 1984.

Composite Inductive Posts in Waveguide—A Multifilament Analysis

GAD S. SHEAFFER, MEMBER, IEEE, AND YEHUDA LEVIATAN, MEMBER, IEEE

***Abstract*—A multifilament moment solution for the analysis of composite dielectric posts in rectangular waveguide is presented. This method permits the analysis of inductive posts composed of disparate regions, each with its own homogeneous complex permittivity. The solution uses the fields generated by sets of fixed-amplitude current filaments to simulate both the field scattered by the posts and the field inside every homogeneous region comprising the posts. Point matching the electric and magnetic fields on the boundaries between regions of different permittivity yields the as yet unknown amplitudes for the current filaments. These currents can in turn be used to calculate field-related parameters of interest such as the scattering matrix and the equivalent circuit parameters. Inductive posts of any shape, composition, size, location, and number can be handled by this method accurately and with very good numerical efficiency. The results obtained are in good agreement with the few cases for which data are available. They also behave well in the limiting cases studied. The solution is further applied to other situations for which no experimental or calculated results are known.**

I. Introduction

The study of dielectric waveguide posts of the inductive type is gaining momentum, with a number of works published. In a recent work by the authors [1], a rapidly converging moment solution for the analysis of homogeneous dielectric posts of the inductive type in rectangular waveguide has been suggested. The solution in [1] is numerically efficient and general in that inductive posts of arbitrary smooth shape, size, location, and number can be handled. It is, however, restricted to homogeneous posts and, furthermore, the formulation introduced there deals explicitly with a single post.

A list of useful references to a large body of work on homogeneous dielectric posts can be found in [1]. Composite posts, that is, posts homogeneous only in parts, have received much less attention. Perhaps the only analysis of anything that can be classified as a composite post problem is the work initiated by Nielsen [2] and pursued by Gotsis, Vafiadis, and Sahalos [3]. In these works, a circular post composed of two concentric regions, each with its own permittivity, was analyzed with the goal of

Manuscript received September 16, 1987; revised November 28, 1987.

G. S. Sheaffer is with OPTOMIC Technologies Corporation Ltd., Science-Based Industrial Park, Technion City, Haifa 32000, Israel.

Y. Leviatan is with the Department of Electrical Engineering, Technion—Israel Institute of Technology, Haifa 32000, Israel.

IEEE Log Number 8719441.

defining a method for measuring the dielectric constant of liquids. However, the method used in [2] and [3] is inherently limited to centered circular posts and cannot be extended to composite posts of general construction.

The study of composite posts is not only of academic interest. A number of practical applications exist. One of them is the method for measuring the dielectric constant of liquids and powders suggested in [3]. Another use can be in hyperthermia treatments, where a patient in a waveguide applicator can be modeled as a dielectric post composed of different regions, whose location and size can be determined by a CT scan [4].

It is the purpose of this paper to expand and generalize the work presented in [1] to handle posts of composite construction. The formulation given here deals with any number of posts, composed of any number of regions of arbitrary shape and location, each with its own complex homogeneous permittivity. Furthermore, posts such as dielectric coated metallic posts, composed of both dielectric and metallic parts, can be handled as well.

II. Problem Specifications

The physical configuration of the problem under study is shown in Fig. 1, together with the coordinate system used. Here, we consider a cylindrical waveguide of rectangular cross section in which a number of composite inductive posts are situated. The width of the guide is a and its height is b. The guide walls are perfect conductors and the guide is filled with a homogeneous medium of constitutive parameters μ_w and ϵ_w. We refer to the waveguide region surrounding the various posts as region w. The posts are composed of a total of M regions with smooth boundaries. We refer to each of these M regions as region p, $p=1,2,\cdots,M$. Each region p is characterized by a permeability μ_p and a permittivity ϵ_p. The various post regions may be lossy; thus μ_p and ϵ_p are in general complex scalars. We denote the boundary surface between the waveguide region and an adjoining post region p by S^{wp} and the boundary surface between adjacent post regions p and q by S^{pq}.

The wave incident upon the post is the dominant TE_{10} mode traveling in the positive z direction. An $\exp(j\omega t)$ time dependence is assumed and suppressed. We confine our consideration to a frequency band within which the TE_{10} is the only propagating mode. Because the electric field vector of the incident mode has only a y component, which is independent of y, and since the properties of the post, both physical and electrical, are uniform along the y direction, the total field in the waveguide does not vary with y. The problem thus reduces to a two-dimensional one.

The objective, in general, is to determine the field scattered by the post and the fields inside the various post regions. Once these fields are known, specific field-related parameters of interest such as the reflection and transmission coefficients, the parameters of the T equivalent network representation for the post two-port junction, and the specific absorption rate (SAR) in the various regions can be readily obtained.

III. Simulated Equivalent Situations

We now divide the original situation into a set of $M+1$ simulated equivalent situations (SES's). An extension of the method suggested in [1] is followed. In the first SES, we simulate the scattered electromagnetic field in region w. In the other M SES's, we simulate the total electromagnetic field in the various homogeneous post regions. In each SES, the simulated field in the corresponding region is generated by a set of current sources

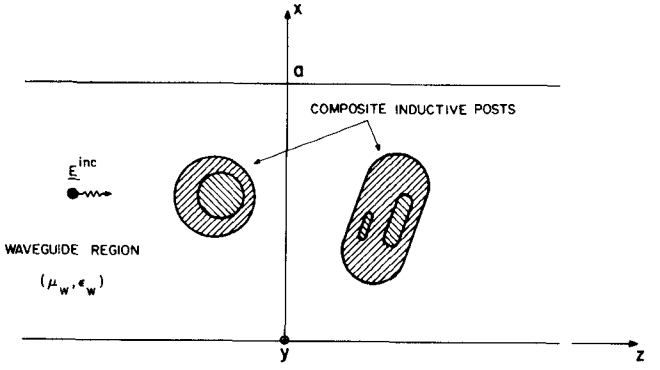

Fig. 1. Composite inductive posts in a rectangular waveguide.

located outside that region. It will be discussed later why some distance from the region boundary is needed. Specifically, in the SES for region w, the physical posts are removed and the field they scatter into the waveguide region is simulated by the field of a set of N^w fictitious filaments of electric current situated in the areas originally occupied by the posts. We denote this field by $(\boldsymbol{E}^w, \boldsymbol{H}^w)$. These filaments are y-directed, extended from top to bottom inside the waveguide, and carry yet to be determined constant complex currents $\{I_i^w\}$, $i=1,2,\cdots,N^w$. They are treated as source currents in a homogeneous waveguide region filled with a medium of constitutive parameters μ_w and ϵ_w. In addition to the field generated by the filamentary sources, the incident field $(\boldsymbol{E}^{\text{inc}}, \boldsymbol{H}^{\text{inc}})$ must be retained in this SES. In the SES for region p, with $p=1,2,\cdots,M$, the total field penetrated into the post region p is simulated by the field of a set of N^p fictitious filaments of electric currents situated around the area originally occupied by region p. These filaments are y-directed, infinite in extent, and carry yet to be determined constant complex currents $\{I_i^p\}$, $i=1,2,\cdots,N^p$. They are treated as source currents in an unbounded space filled with homogeneous material identical to the one composing post region p. Expressions for the incident TE_{10} field $(\boldsymbol{E}^{\text{inc}}, \boldsymbol{H}^{\text{inc}})$ and for the fields $(\boldsymbol{E}^w, \boldsymbol{H}^w)$ and $(\boldsymbol{E}^p, \boldsymbol{H}^p)$, $p=1,2,\cdots,M$, will not be made explicit here. They can be found in [1, sec. IV].

The electromagnetic fields in the various SES's are related by the continuity conditions on the boundaries between them. Specifically, these fields have to satisfy the following equations:

$$\left.\begin{aligned}\hat{\boldsymbol{n}}\times(\boldsymbol{E}^p-\boldsymbol{E}^w)&=\hat{\boldsymbol{n}}\times\boldsymbol{E}^{\text{inc}}\\ \hat{\boldsymbol{n}}\times(\boldsymbol{H}^p-\boldsymbol{H}^w)&=\hat{\boldsymbol{n}}\times\boldsymbol{H}^{\text{inc}}\end{aligned}\right\}\quad \text{on each } S^{wp} \tag{1}$$

$$\left.\begin{aligned}\hat{\boldsymbol{n}}\times(\boldsymbol{E}^p-\boldsymbol{E}^q)&=0\\ \hat{\boldsymbol{n}}\times(\boldsymbol{H}^p-\boldsymbol{H}^q)&=0\end{aligned}\right\}\quad \text{on each } S^{pq} \tag{2}$$

where $\hat{\boldsymbol{n}}$ is a unit vector normal to the respective surface. If current sources for every SES were found which satisfy (1) and (2), then the field in each SES would be equal to the exact field in that respective region in the original situation. Our solution uses a finite set of sources whose fields, due to the distance between them and the boundary surfaces, constitute a basis of smooth field functions suitable for representing fields on the smooth boundary surfaces. The key advantage here is that we represent smooth quantities on the various boundary surfaces using sources whose fields are known analytically, thereby avoiding laborious surface current integrations when computing the fields at the various stages of the solution. Furthermore, since the fields on the various boundaries are actually represented by means of smooth expansion functions, a simple point-matching procedure can be adopted for testing (1) and (2). Of course, being numeri-

cal, the solution is never exact. Our objective is thus to approximate the fields to some desired accuracy. The solution can be verified by checking the degree to which the required boundary conditions are satisfied over a denser set of points on the boundary. This is easily accomplished as field calculations are summations of trivial analytic terms. Clearly, the boundary condition check can immediately point out results that are definitely inaccurate. In addition, for lossless posts, the unitary condition, which must be satisfied by the scattering matrix, can provide an even simpler and faster check.

IV. Formulation

Following the above-outlined procedure, the functional equations of (1) for each boundary surface S^{wp} reduce to the matrix equations

$$[Z_e^p]\vec{I}^p - [Z_e^w]\vec{I}^w = \vec{V}_e \tag{3a}$$

$$[Z_h^p]\vec{I}^p - [Z_h^w]\vec{I}^w = \vec{V}_h. \tag{3b}$$

Similarly, the functional equations of (2) for each boundary surface S^{pq} reduce to the matrix equations

$$[Z_e^p]\vec{I}^p - [Z_e^q]\vec{I}^q = 0 \tag{4a}$$

$$[Z_h^p]\vec{I}^p - [Z_h^q]\vec{I}^q = 0. \tag{4b}$$

In (3a), $[Z_e^p]$ and $[Z_e^w]$ are generalized impedance matrices whose (l, i) elements are, respectively, the electric field intensities E_{ly}^p due to a filament I_i^p of unit current and E_{iy}^w due to a filament I_i^w of unit current, both evaluated at (x_l, z_l) on S^{wp}; $\vec{I}^p$ and $\vec{I}^w$ are column vectors whose ith elements are, respectively, I_i^p and I_i^w; and $\vec{V}_e$ is a column vector whose lth element is E_y^{inc} at observation point (x_l, z_l) on S^{wp}. In (3b), $[Z_h^p]$ and $[Z_h^w]$ are generalized impedance matrices whose (l, i) elements are, respectively, the tangential magnetic field intensities due to a filament I_i^p of unit current and due to a filament I_i^w of unit current, both evaluated at (x_l, z_l) on S^{wp}; and $\vec{V}_h$ is a column vector whose lth element is the tangential magnetic field intensity of the incident wave at observation point (x_l, z_l) on S^{wp}. Finally, in (4a) and (4b), the various matrices are defined in a manner similar to the definitions above with the observation points taken on S^{pq}.

The $2(M+1)$ matrix equations in (3) and (4) can now be combined to form a single matrix equation of the form

$$[Z]\vec{I} = \vec{V}. \tag{5}$$

This matrix equation is solved for the unknown filamentary currents by inversion or elimination. Once the filamentary currents are known, the solution of the problem is completed as the fields in regions of interest and field-related quantities of interest can be readily evaluated by trivial summations.

V. Numerical Results

The results given in this section will be of three types. First, a comparison will be made with other known results. Second, the results for a few limiting cases will be given. Finally, data for some cases for which no other results are available will be presented.

A case that can be classified as a composite post problem is given in [3]. The case analyzed there is a post made up of two concentric layers. The outer layer is a glass test tube of 3.34 mm outer radius and 2.38 mm inner radius and with permittivity of $3.78\epsilon_0$. The inner layer is a liquid column whose complex permittivity $\epsilon_0(\epsilon_r - j\epsilon_i)$ is to be determined. A graph for determining that permittivity, based on the results of measurement at 10 GHz in a WR 90 waveguide, is given in [3] and is replicated in Fig. 2 using results generated by our method. The results are identical. Note that in order to determine both the real and the imaginary part of the tested permittivity it is necessary to measure two parameters. These parameters can be, for example, the magnitude $|T|$ and phase ϕ_T of the transmission coefficient, as in the case of Fig. 2. It would, however, be considerably easier to measure only a single parameter such as the magnitude of the reflection coefficient. This would require only a scalar network analyzer and a one-port measurement. A measurement of the reflection coefficient at two different locations of the post, for example, when the post is centered and when it is offset (along the x axis), can also yield data sufficient to determine the complex permittivity of the material under test. This latter technique is not possible with the method described in [3] as this method can handle only centered posts. It is, however, possible with the method described here, since posts at any location can be handled.

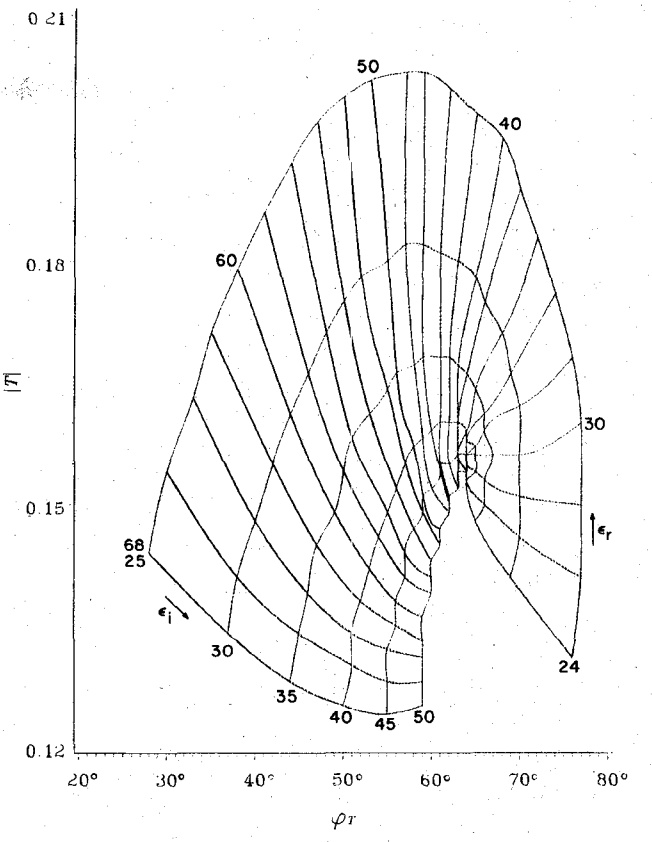

Fig. 2. Plots of magnitude and phase of the transmission coefficient T as a function of the complex permittivity $\epsilon_0(\epsilon_r - j\epsilon_i)$ at 10 GHz for a dielectric core inside a glass test tube. The width of the guide is $a = 22.86$ mm. The dielectric core is of 2.38 mm radius. The surrounding glass tube is of 3.34 mm outer radius and with permittivity of $3.78\epsilon_0$.

The study of limiting cases has a twofold advantage. It permits the verification of the theory involved and at the same time provides a check on the accuracy of the computer program written based on that theory. Fig. 3 illustrates some of the limiting cases studied. Both a dielectric shell and a solid dielectric post are studied. To better test the program, the results for the solid post are actually the results of a post composed of two concentric layers, both with the same electrical parameters, a limiting case in itself. In both the solid post case and the dielectric shell case, the inner radius (the radius of the inner layer

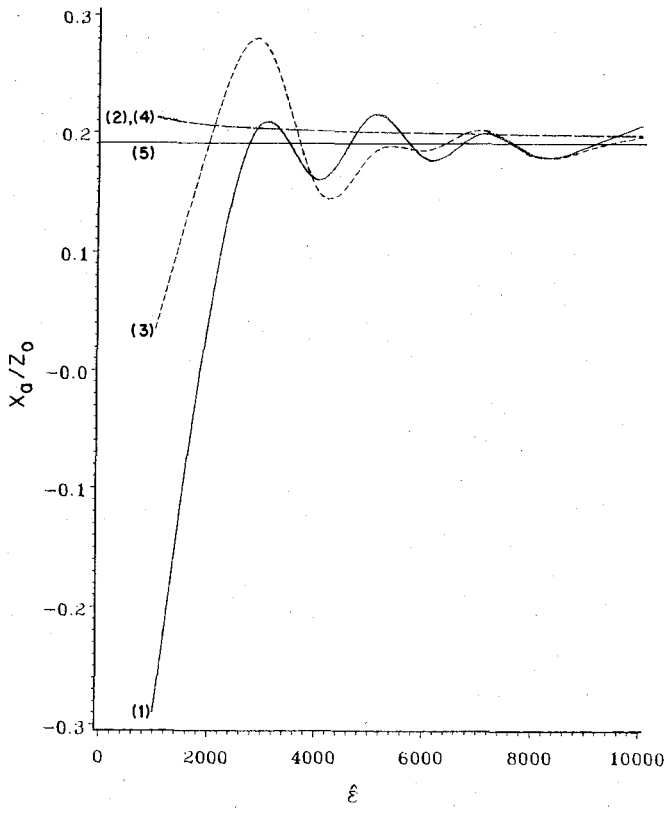

Fig. 3. Plots of normalized parallel reactance X_a/Z_0 of the equivalent T network versus the parameter $\hat{\epsilon}$ for the following cases: (1) solid dielectric post of permittivity $\epsilon_0(\hat{\epsilon}-j0)$; (2) solid dielectric post of permittivity $\epsilon_0(1-j\hat{\epsilon})$; (3) dielectric shell of permittivity $\epsilon_0(\hat{\epsilon}-j0)$; (4) dielectric shell of permittivity $\epsilon_0(1-j\hat{\epsilon})$; and (5) metallic post (perfectly conducting). The solid post is of radius $0.1a$, the shell is of inner radius $r_{\text{in}}=0.05a$, and thickness $t=0.05a$ ($a=\lambda/1.4$).

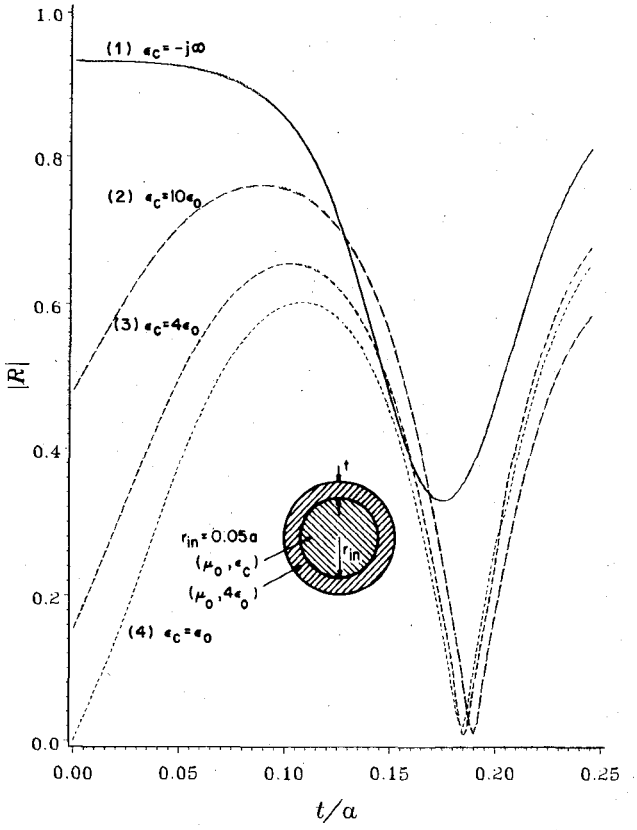

Fig. 4. Plots of the magnitude of the reflection coefficient R as a function of the shell thickness t for a dielectric shell of permittivity $4\epsilon_0$ surrounding various inner cores of radius $0.05a$ ($a=\lambda/1.4$). Cases treated are (1) perfectly conducting core; (2) core of permittivity $\epsilon_c=10\epsilon_0$; (3) core of permittivity $\epsilon_c=4\epsilon_0$ (identical to that of the outer layer); and (4) core of permittivity $\epsilon_c=\epsilon_0$ (free space).

in the case of the solid post) is $r_{\text{in}}=0.05a$. The outer layer is of thickness $t=0.05a$. Here, $\lambda=1$ m and $a=\lambda/1.4$. For all cases the real and imaginary parts of the dielectric constant were given (one at a time) increasingly large values, with the goal of approximating a metallic post. The figure shows plots of the normalized parallel reactance X_a/Z_0 of the T equivalent network representation [1] versus the parameter $\hat{\epsilon}$ for the following discontinuities: (1) solid dielectric post of permittivity $\epsilon_0(\hat{\epsilon}-j0)$; (2) solid dielectric post of permittivity $\epsilon_0(1-j\hat{\epsilon})$; (3) dielectric shell of permittivity $\epsilon_0(\hat{\epsilon}-j0)$; (4) dielectric shell of permittivity $\epsilon_0(1-j\hat{\epsilon})$; and (5) metallic post (perfectly conducting). As is evident from Fig. 3, for large values of either the real or the imaginary part of the dielectric constant, the results for a metallic post are retrieved.

The versatility of the present method is evident from the data presented in Fig. 4. In the four cases studied, a dielectric shell with permittivity of $4\epsilon_0$ and varying thickness t surrounds a core of $0.05a$ radius. The outer shell thickness t varies between 0 and $0.25a$. Here, $a=\lambda/1.4$. The inner core in graphs 1–4 is composed, respectively, of a perfectly conducting material, a dielectric of permittivity $\epsilon_c=10\epsilon_0$, a dielectric of permittivity $\epsilon_c=4\epsilon_0$ (identical to that of the outer layer), and free space $\epsilon_c=\epsilon_0$. Thus the four cases studied are (1) dielectric-coated metallic post, (2) dielectric post composed of two concentric layers of contrasting permittivities, (3) solid dielectric post, and (4) dielectric shell. Notice the resonance in the last three cases that occurs when the thickness of the outer layer is about $0.19a$. The reflection then is very close to zero, even though the post blocks almost half the width of the waveguide. Similar resonance behavior can be found for homogeneous posts in [5] and [6].

VI. Application Notes

In order to ease the application of the previously given general formulation, a few guidelines are offered. The two main issues for a successful application of the method are the location and the number of both the sources and the matching points.

Location of Matching Points: These points will in general be equally spaced. A nonuniform spacing might, however, be advantageous in certain situations, and there is an incentive to use more matching points in areas where the field is expected to vary rapidly. In most cases the same points will be used for matching both the electric and the magnetic fields. That, however, is not mandatory and different matching points for the electric and magnetic fields might sometimes be useful. In most of the cases studied by us, separating the matching points did not yield any noticeable improvement, and for convenience these points were chosen to coincide.

Location of Current Sources for a Specific Region: These will be outside that region, at a certain distance from the boundary. From both intuition and experience, the optimal location for the sources is on a contour of the same shape as, and concentric with, the region boundary. In the case of an annular region with an inner radius r_{in} and an outer radius r_{out}, for instance, the sources will be located on two contours, both circular in shape. One contour will be of radius $0.5r_{\text{in}}$ and the other of radius $2r_{\text{out}}$. It should be noted that this choice is only a recommendation as the suggested method is relatively insensitive to this parameter, provided the sources are sufficiently distant from the boundary. As to the placement of the sources on that contour, as long as the boundary is smooth, uniformly spacing the sources on the con-

tour is both simple and numerically efficient. For less regular boundaries, a good practice would be to locate more sources in the vicinity of the irregularities in the contour's shape and have these sources closer to the boundary.

Number of Sources and Matching Points: Let us denote by N_s the number of sources in the SES for a certain region. Also, let N_e and N_h be, respectively, the number of matching points for the electric and magnetic fields on the region's boundary. Having $N_s = N_e = N_h$ for each SES is quite convenient and useful in most cases, but is not mandatory. The only restriction is that the total number of matching points (notice that each matching point is common to two adjacent regions) be equal to or larger than the total number of sources so as to have a sufficient number of equations. Despite the freedom afforded by the above, the size, shape, and composition of the region should be taken into consideration when setting N_s, N_e, and N_h. For metallic regions, since only the electric field has to be matched (to zero) at the boundary, let $N_s = 0$ and $N_h = 0$. The number N_e is a function of the curvature and the length of the boundary. If the radius of curvature is smaller than $\lambda/5$, one should fix the matching points approximately half the radius of curvature apart. On the other hand, if the radius of curvature is larger than $\lambda/5$, one should consider about ten matching points per wavelength. For dielectric regions, the number of matching points $N_e = N_h$ is also a function of the boundary curvature and length. Again, if the radius of curvature is smaller than $\lambda/5$, one should fix the matching points approximately half the radius of curvature apart. On the other hand, if the radius of curvature is larger than $\lambda/5$, one should consider about ten matching points per wavelength in the region. Thus, a region of a higher permittivity would usually require more matching points. The number of sources can be equal to the number of matching points.

References

[1] Y. Leviatan and G S. Sheaffer, "Analysis of inductive dielectric posts in rectangular waveguide," *IEEE Trans. Microwave Theory Tech*., vol. MTT-35, pp. 48–59, Jan. 1987.

[2] E. D. Nielsen, "Scattering by a cylindrical post of complex permittivity in a waveguide," *IEEE Trans. Microwave Theory Tech*., vol. MTT-17, pp. 148–153, Mar. 1969.

[3] N. Gotsis, E. E. Vafiadis, and J. N Sahalos, "The discountinuity problem of a cylindrical dielectric post in a waveguide and its application on the dielectric constant measurements of liquids," *Archiv fur Elektrotechniks*, vol. 68, pp. 249–257, 1985.

[4] S. Mizushina, Y. Xiang, and T. Sugiura, "A large waveguide applicator for deep regional hyperthermia," *IEEE Trans. Microwave Theory Tech*., vol. MTT-34, pp. 644–648, May 1986.

[5] J. N. Sahalos and E. Vafiadis, "On the narrow-band microwave filter design using a dielectric rod," *IEEE Trans. Microwave Theory Tech* , vol. MTT-33, pp. 1165–1171, Nov. 1985.

[6] C. G. Hsu and H. Auda, "Multiple dielectric posts in a rectangular waveguide," *IEEE Trans. Microwave Theory Tech*., vol. MTT-34, pp. 883–891, Aug. 1986.

TE–TM Mode Conversion of an Optical Beam Wave in Thin-Film Optical Waveguides

KAZUNORI HANO

***Abstract*—This paper describes the TE–TM mode conversion efficiency when a Gaussian beam wave propagates in thin-film optical waveguides. For film thicknesses at which strong coupling between the TE and TM modes is obtained, two hybrid modes have oppositely rotating circular polarizations, or linear polarizations perpendicular to each other with equal magnitude of TE and TM wave components. In the former (i.e., circular polarization), complete TE–TM mode conversion is impossible. In the latter (i.e., linear polarization) complete TE–TM mode conversion is available. These claims are based on the fact that the direction of power flow of the hybrid modes depends on the polarization.**

Manuscript received September 22, 1987; revised November 23, 1987.

The author is with the Department of Electronics, Faculty of Engineering, Kyushu Institute of Technology, Tobata-ku, Kitakyushu, 804 Japan.

IEEE Log Number 8719442.

I. Introduction

Many studies have been made on thin-film optical waveguide devices utilizing the principle of TE–TM mode conversion, such as optical switches, modulators, and circulators [1]–[9]. For efficient TE–TM mode conversion, phase matching between the TE and TM modes is required. For this purpose, anisotropic media are used in part (or all) of the waveguide.

In general, the eigenmodes of the waveguide containing anisotropic media are hybrid modes. The phenomenon of the TE–TM mode conversion can be described as coupling between two hybrid modes [5], [6]. But, the direction of power flow of the hybrid modes is generally different from that of the wave-normal (a phenomenon called "walk off") [7]–[10]. Moreover, the direction of power flow of one of the two hybrid modes is not always the same as that of the other mode [11]. Therefore, when an optical beam wave is employed in the TE–TM mode conversion, it is expected that the coupling between the two hybrid modes gradually ceases as they travel down the waveguide even if both wave-normals are in the same direction. But, the conversion efficiency taking into account these effects has not been reported so far.

In this short paper we investigate TE–TM mode conversion efficiency when a Gaussian beam wave propagates in a thin-film optical waveguide with uniaxial anisotropic substrates. The diffraction of the beam wave is neglected. The uniaxial anisotropic substrates are gyrotropic or anisotropic media, and the dielectric tensor has longitudinal or polar configuration [1]. As the analysis of the hybrid modes in the thin-film waveguides has been reported [2], [5]–[10], only the conversion efficiency is given. It will be shown that complete TE–TM mode conversion is impossible for circularly polarized hybrid modes and that complete TE–TM mode conversion is available for linearly polarized hybrid modes.

II. TE–TM Mode Conversion

Fig. 1 shows a thin-film optical waveguide consisting of three sections: I (input), II (converter), and III (output). The top layer and film are lossless isotropic dielectric media with refractive indices of n_t and n_f, respectively. The substrate is a lossless uniaxial anisotropic dielectric medium having ordinary and extraordinary refractive indices of n_o and n_e, respectively. The permeabilities of the three media are equal to μ_0 (permeability of vacuum). The optic axis of the uniaxial anisotropic medium is parallel to the y axis for $z < 0$ and $l < z$, but is at an angle ζ with respect to the y axis for $0 < z < l$, as shown in Fig. 1. Then, the eigenmodes are TE and TM modes in sections I and III, and are hybrid modes in section II. The film thickness of the waveguide is taken to $d = d_0$, at which TE_0 and TM_0 modes are degenerate in sections I and III and two hybrid modes H_0^+ and H_0^- can propagate in section II. At the film thickness d_0, the two H_0^+ and H_0^- modes have right- and left-handed circular polarizations for longitudinal gyrotropic and polar anisotropic cases, or linear polarizations perpendicular to each other with equal magnitude of the TE and TM wave components for longitudinal anisotropic and polar gyrotropic cases [2]. Here, the direction of power flow

0018-9480/88/0400-0783$01.00 ©1988 IEEE